Crystallographic characterization of epitaxial $Pb(Zr,Ti)O_3$ films with different Zr/Ti ratio grown by radio-frequency-magnetron sputtering

Isaku Kanno[a] and Hidetoshi Kotera
Department of Mechanical Engineering, Kyoto University, Kyoto 606-8501, Japan

Kiyotaka Wasa
Faculty of Science, Yokohama City University, Yokohama 236-0027, Japan

Toshiyuki Matsunaga, Takeshi Kamada, and Ryouichi Takayama
Matsushita Electric Industry, Osaka 570-8501, Japan

(Received 17 June 2002; accepted 16 January 2003)

Crystallographic structure of as-grown epitaxial $Pb(Zr,Ti)O_3$ (PZT) films was investigated with regard to the Zr/Ti ratio and crystalline orientation. PZT films with (001) and (111) orientation were epitaxially grown on (100) and (111)$SrTiO_3$ substrates respectively using radio-frequency (rf) sputtering. Four circle x-ray diffraction measurements revealed that the crystallographic dependence on Zr/Ti composition in PZT films was much different from bulk PZT. In particular, (001)-oriented PZT films showed tetragonal structure even in the Zr/Ti composition of 70/30 where the bulk PZT ceramics are rhombohedral phase. In addition, although (001)-oriented PZT films with Zr/Ti ratio of 53/47 and 70/30 showed tetragonal structure, (111)-oriented PZT films with the same Zr/Ti ratio were identified as the rhombohedral structure. The cell volume of the PZT films with both orientations increased, suggesting the excess Pb atoms in the films due to the impinging energetic sputtered particles induces the anomalous crystalline structure of the PZT films. Dielectric properties of the PZT films exhibited stable value independent of Zr/Ti ratio and characteristic increase of dielectric constant near Zr/Ti=53/47 could not be observed. These results suggest that the internal stress due to the sputter deposition plays an important roll in the unique characteristics of crystallographic and electrical properties of the epitaxial PZT films. © *2003 American Institute of Physics.* [DOI: 10.1063/1.1558951]

I. INTRODUCTION

Investigation of the ferroelectric thin films has been of importance for various applications such as nonvolatile random access memories[1] and micropiezoelectric sensors/actuators in microelectromechanical systems (MEMS).[2–7] For MEMS applications, $Pb(Zr,Ti)O_3$ (PZT) thin films are considered to be the most promising materials due to their excellent ferroelectric and piezoelectric characteristics.[8–10] It is well-known that the polycrystalline PZT ceramics exhibit their highest dielectric and piezoelectric properties in the composition near the morphotoropic phase boundary around Zr/Ti=53/47. Most of the PZT films have been fabricated in polycrystalline structure because the deposition is often carried out using nonepitaxial substrates like silicon for their applications to the monolithic integrated devices. On the other hand, single crystal PZT films could be epitaxially grown using single crystal substrates like $SrTiO_3$ (STO) and MgO, and enhancement of piezoelectric properties could be expected by the optimization of the crystalline orientation of the PZT films.[11–13] Preparation of epitaxial PZT films has been performed using several techniques such as rf-magnetron sputtering,[11,14] metalorganic chemical vapor deposition (MOCVD),[15,16] and pulsed laser ablation.[17] Epitaxial PZT films, however, are considered to be suffering large internal stress due to the restriction from the substrates, leading to the obvious distortion of electric properties as well as crystalline structure from the bulk ceramics. For the MEMS devices, evaluation and control of the internal stress of the PZT films are important in the microfabrication and prediction of resulting electric properties. Although the stress-induced deformation of the crystalline structure as well as the dielectric properties has been discussed in several articles,[14,18,19] there is still a lack of knowledge on the effects of the epitaxial orientation of the PZT films.

In this study we have prepared epitaxial PZT films with (001) and (111) orientations and evaluated the crystalline structure in detail, varying their Zr/Ti composition from 40/60 to 70/30. From the viewpoint of MEMS applications as micropiezoelectric devices, relatively thick PZT films more than 2 μm were deposited on Pt-coated STO substrates and estimated dielectric and ferroelectric properties. In this article we discuss the combined effects of PZT film composition and orientation on the crystallographic structure and their electric properties.

II. EXPERIMENT

PZT thin films were prepared by the rf-magnetron sputtering technique which has several advantages such as excellent stability of film composition and structure, smooth surface morphology, and stable growth rate compared with the other epitaxial growth methods. Typical sputtering conditions

[a]Electronic mail: kanno@mech.kyoto-u.ac.jp

 © 2003 American Institute of Physics

Downloaded 06 Mar 2008 to 130.54.110.22. Redistribution subject to AIP license or copyright; see http://jap.aip.org/jap/copyright.jsp

TABLE I. Growth conditions of the PZT films.

Substrate	(100)Pt/(100)$SrTiO_3$
	(111)Pt/(111)$SrTiO_3$
Substrate temperature	550 °C
Gas	Ar/O_2
Pressure	0.3–0.5 Pa
Target	$[Pb(Zr_xTi_{1-x})O_3]_{0.8}+[PbO]_{0.2}$
	$x=0.40$, 0.53, 0.70
Film thickness	Pt: ~0.1 μm
	PZT: 2.5–3.0 μm

were listed in Table I. Substrates used were (100) and (111)STO single crystal. In order to examine electrical properties of the PZT films, Pt bottom electrodes of 100 nm in thickness were epitaxially grown on the STO substrates by rf sputtering prior to the deposition of the PZT films. The PZT sputter depositions were conducted under the Ar/O_2 mixed gas atmosphere of 0.3–0.5 Pa. PZT thin films were grown on the (100)Pt/(100)STO and (111)Pt/(111)STO substrates which were heated around 550 °C and no thermal treatments such as postannealing were performed for the resulting films. We deposited PZT films with relatively high growth rate of 1.0–1.2 μm/h and resulting thickness was 2.5–3.0 μm. After the deposition was completed, PZT films were naturally cooled from deposition temperature down to room temperature in vacuum chamber for about 3 h. Three types of the ceramic targets with different Zr/Ti ratio of 40/60, 53/47, and 70/30 were used in order to examine influences of orientation and Zr/Ti composition on the crystallographic structure of the PZT films. Excess PbO was added into the every target for the compensation of the lead re-evaporation from the films.

The film composition was determined using electron probe microanalysis. The wavelength dispersive x-ray (WDX) spectrometry measurements were carried out for PZT films epitaxially grown on (100)MgO substrates in order to eliminate the influence of Ti element of the STO substrates. For each target, we confirmed that the Zr/Ti ratio of the deposited PZT films was almost same as that of the target within the deviation less than 3%. Therefore, we identified the film composition of Zr/Ti with the target Zr/Ti ratio. On the other hand, Pb concentration of Pb/(Zr+Ti) ratio was about 1.05–1.10, indicating the PZT films contained excess Pb probably due to the impinging the sputtered Pb atoms with high kinetic energy onto the growing films. Crystalline structure of as-grown PZT films was investigated by x-ray diffraction measurements. In order to identify the crystallographic phase of the PZT films, reciprocal space analysis was carried out by four circle diffractmeter (Phillips X'Pert) using Cu *K*a emission. For the PZT films grown on (100)Pt/(100)STO, lattice parameters of (100) and (001) were calculated from the peak positions of (204) and (004)PZT reflections in the reciprocal lattice maps. For the PZT films grown on (111)Pt/(111)STO, on the other hand, (330) and (005)PZT reflections were used for the calculation of the lattice parameters of the PZT films.

The relationship between the crystalline structure of the epitaxial PZT and the electric properties was examined using

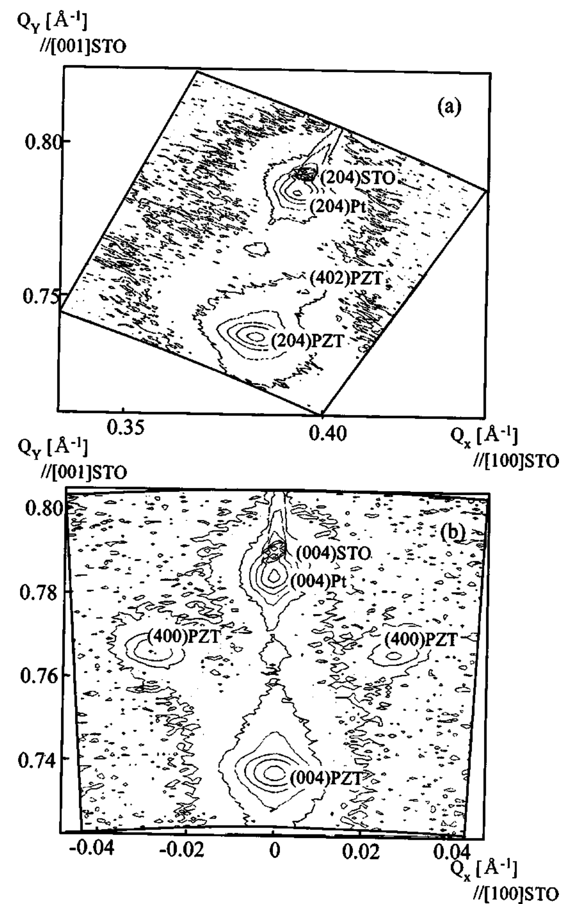

FIG. 1. Contour maps of reciprocal lattice of the PZT films (40/60) grown on (100)Pt/(100)STO; (a) (204)PZT and (b) (004)PZT diffractions. STO and Pt diffractions were also observed for the reference data. 90° domain structure of the PZT films could be clearly observed.

Au top electrode with 0.5 mm in diameter. The dielectric constant was evaluated using impedance analyzer (HP4192A). *P–E* hysteresis loops of the PZT films were measured by a conventional Sawyer–Tower circuit. We investigated the influence of unique crystalline structure of the PZT films on the electric properties as a function of Zr/Ti ratio.

III. RESULTS

In order to characterize morphotoropic phase transition of the PZT in the film form, analysis of reciprocal lattice was carried out. Figure 1 shows the diffraction contour maps of (004) and (204)PZT with Zr/Ti of 40/60 grown on (100)Pt/(100)STO. The measurement revealed that the PZT films were epitaxially grown on the substrates. In Fig. 1(b), not only strong (004)PZT peak but (400)PZT peaks were clearly observed, indicating the PZT films were oriented along *c* axis with the 90° domain structure. Lattice constants of the PZT films were calculated from the peak positions of the reciprocal lattice maps as listed in Table II. For the PZT films of 40/60 grown on (100)STO, the lattice constants were derived from the peak positions of *a* and *c* domains, respectively. It should be noted that the lattice constants show slightly different values between *a* and *c* domains. The *a* axis in the *c* domain is longer than that in *a* domain, and alternatively, *c*

Downloaded 06 Mar 2008 to 130.54.110.22. Redistribution subject to AIP license or copyright; see http://jap.aip.org/jap/copyright.jsp

TABLE II. Lattice constants of the PZT films grown on (100)STO. The values were derived from the peak positions of the reciprocal lattice maps of (204) and (004) PZT diffractions. Lattice constants of the *a* and *c* axes represent parallel and normal spacings to the substrate individually.

PZT (Zr/Ti)	Domain	*a* axis (Å)	*c* axis (Å)
40/60	*a* domain	4.019	4.190
	c domain	4.030	4.179
53/47	*c* domain	4.066	4.145
70/30	*c* domain	4.085	4.146

TABLE III. Calculated lattice constants of the PZT films grown on (111)STO. The values were derived from the peak positions of the reciprocal lattice maps of (330) and (005) PZT diffractions.

PZT (Zr/Ti)	*a* axis (Å)	*c* axis (Å)
40/60	4.041	4.143
53/47	4.087	4.088
70/30	4.107	4.116

axis in the *c* domain is smaller than that in the *a* domain, that is, the lattice constant parallel to the substrate is larger than that normal to the substrate. These results represent that the PZT films suffer slight in-plain stress from the substrates. On the other hand, for the PZT films of 53/47 and 70/30, similar reciprocal lattice maps were observed, but no domain structure could be identified. Additionally, calculated lattice constants of both PZT films show the larger *c* axis (out-of-plane spacing) than the *a* axis (in-plane spacing) even in the Zr/Ti ratio of 70/30 where PZT ceramics show rhombohedral structure.

Similar analysis of the crystalline structure of the PZT films grown on (111)Pt/(111)STO was carried out using (005) and (330)PZT diffraction spots. Figure 2 shows the reciprocal lattice maps of (005) and (330) of the PZT films of 53/47. The measurements revealed that the PZT films were epitaxially grown with the relationship of (111)PZT//(111)Pt//(111)STO. Although almost similar patterns were observed for PZT films of 40/60 and 70/30, in the case of Zr/Ti=40/60 the peak patterns became broader and split of the diffraction peak was clearly observed in the (005)PZT, indicating the *c*/*a* domain structure existed in the film. The calculated lattice constants of the PZT films grown on (111)Pt/(111)STO were listed in Table III. Judging from the fact that the lattice constants of *a* and *c* axes for the (111)-oriented PZT films of 53/47 and 70/30 exhibit almost same values, it could be considered that these PZT films are rhombohedral structure. The lattice constants of the epitaxial PZT films are plotted in Fig. 3 as a function of the Zr/Ti composition. This result demonstrated that the phase diagram of the epitaxial PZT films is substantially distorted from that of bulk PZT,[20] and furthermore, it also depends on the orientation of the PZT films.

In order to investigate the relationship between anomalous crystalline structure and electric properties, dielectric properties of the PZT films were measured. Figure 4 shows the relative dielectric constant of the PZT films as a function of Zr/Ti ratio. The measurements revealed that the dielectric constants of the (111)-oriented PZT films were higher than (001)-oriented ones. In addition, the difference on film orientations decreased as the Zr/Ti ratio increased. However, significant increase of the dielectric constant near Zr/Ti =53/47 could not be observed.

P–E hysteresis loops of the PZT films were shown in Fig. 5. All films exhibited asymmetric loops with larger positive coercive electric field ($+E_c$) than negative coercive

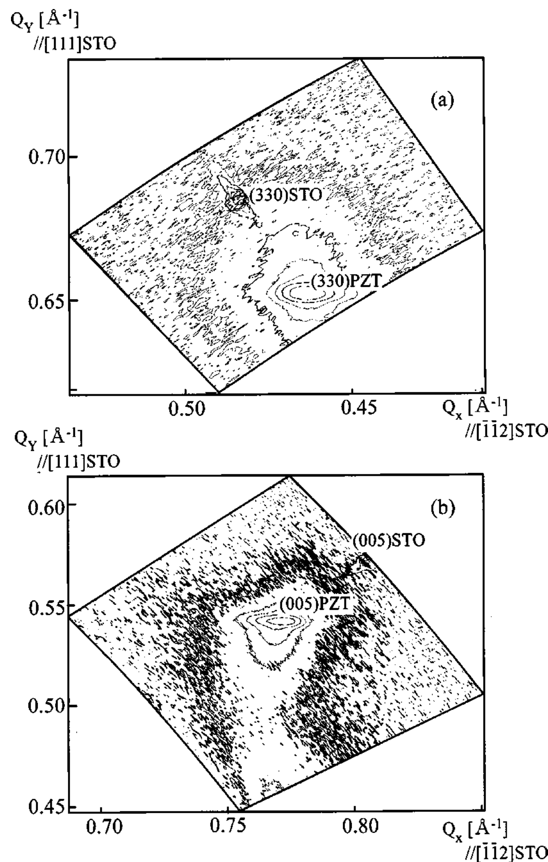

FIG. 2. Contour maps of reciprocal lattice of the PZT films (53/47) grown on (111)Pt/(111)STO; (a) (330)PZT diffraction and (b) (005)PZT diffraction. Peak split due to the domain structure could not be observed.

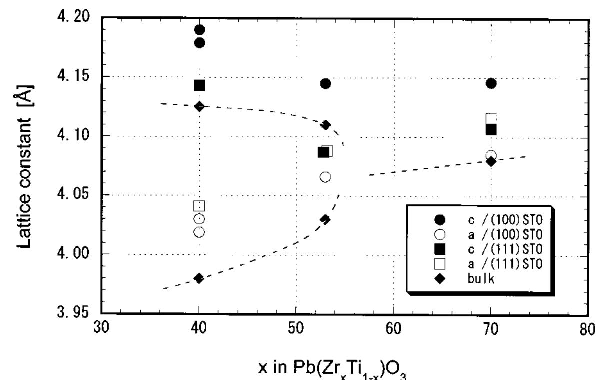

FIG. 3. Lattice constants of the PZT films as a function of Zr/Ti ratio. ● and ○ represent the *c*- and *a*-lattice constants of PZT films grown on (100)Pt/(100)STO, respectively. ■ and □ also represent the *c*- and *a*-lattice constants of PZT films grown on (111)Pt/(111)STO, respectively. For the PZT films of Zr=40% grown on (100)Pt/(100)STO, two sets of lattice constants are plotted according to domain structure as listed in Table II. ◆ and dashed line indicate the bulk data (see Ref. 20).

Downloaded 06 Mar 2008 to 130.54.110.22. Redistribution subject to AIP license or copyright; see http://jap.aip.org/jap/copyright.jsp

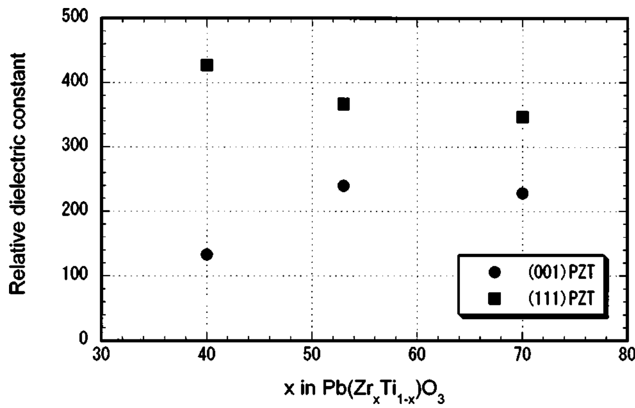

FIG. 4. Relative dielectric constants of the PZT films as a function of Zr/Ti ratio. ● and ■ represent the values of (001)PZT and (111)PZT films, respectively.

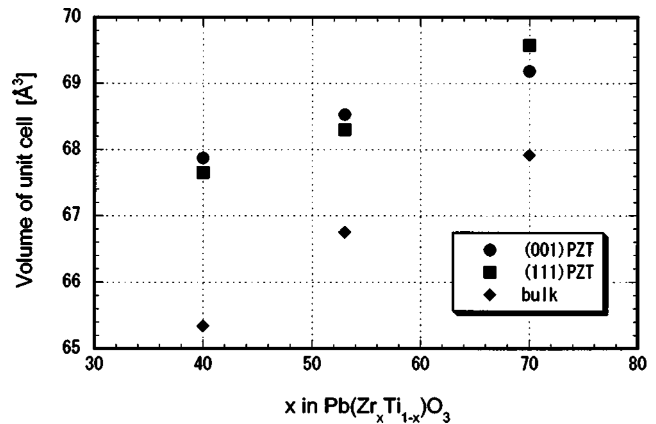

FIG. 6. Volume of the PZT unit cell as a function of the Zr/Ti ratio. ● and ■ represent the values of (001)PZT and (111)PZT films, respectively. Bulk data are plotted as ◆.

electric field ($-E_c$). Such asymmetry of the *P–E* hysteresis loops could be explained by the space charge trapped at electrode and PZT films.[21] On the other hand, the hysteresis loops of (001)-oriented PZT films showed clear rectangular shape, while the E_c and remanent polarization (P_r) decrease with increasing Zr concentration. However, the shape of hysteresis loops did not show remarkable compositional dependence like bulk PZT. In the case of the (111)-oriented PZT films, *P–E* hysteresis loops were almost independent of the film composition and stable ferroelectricity was observed.

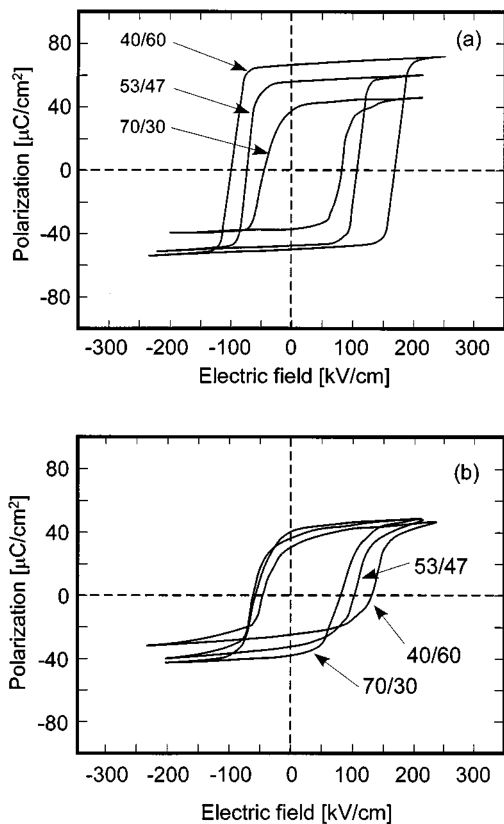

FIG. 5. *P–E* hysteresis loops of PZT films with Zr/Ti ratio of 40/60, 53/47, and 70/30; (a) (001)-oriented PZT films, and (b) (111)-oriented PZT films.

IV. DISCUSSION

The crystallographic analysis of the epitaxial PZT thin films demonstrated that the phase diagram of the PZT thin films was substantially distorted from that of polycrystalline bulk ceramics. Furthermore, phase diagram of the PZT films was remarkably influenced by the epitaxial orientation. The crystallographic difference of the PZT between thin films and bulk ceramics is attributed to the internal film stress, which might be generated by not only thermal expansion and lattice mismatch between PZT and substrate, but also sputter-induced defects like anomalous positioning of component atoms. The thermal stress is caused by the difference of the thermal expansion coefficients between PZT thin films and STO substrates, where contribution of Pt electrode could be neglected due to its thin thickness of 0.1 μm. After the deposition is completed, PZT films suffer large temperature difference during cooling down from the deposition temperature about 550 °C to a room temperature. It was reported that the thermal expansion coefficients of PZT and STO were almost the same value ($\sim 11\times 10^{-6}$ °C),[17] indicating that it might not be the main reason of the anomalous crystalline structure of the PZT films. Another possibility is the phase transition during cooling process. In the case of the PZT in the tetragonal phase, both *c*-axis elongation and *a*-axis contraction take place below the Curie temperature (T_c), so that large tensile stress might be imposed on the *c*-axis oriented PZT films from the STO substrates. This in-plane stress may cause the slight difference of lattice constants between *a* and *c* domain of the PZT films of 40/60 grown on (100)Pt/(100)STO as mentioned earlier. However, although the effect of thermal stress corresponds with the elongation of *a* axis of the PZT films of 40/60 and 53/47, the lattice constants of the *c* axis show 4.179 Å (40/60) and 4.145 Å (53/47), respectively, which are also larger than those of bulk PZT as shown in Fig. 4. Figure 6 shows the cell volume of the PZT films and bulk ceramics[20] as a function of the Zr/Ti ratio. The volume of every PZT film increases about 2%–3.5% from bulk one, but it is difficult to explain such large swelling of

Downloaded 06 Mar 2008 to 130.54.110.22. Redistribution subject to AIP license or copyright; see http://jap.aip.org/jap/copyright.jsp

the cell volume only by the interfacial forces between PZT films and STO substrates such as thermal stress and lattice mismatch.

Another possible reason of the elongation of both *a* and *c* axes is sputter-induced effects on the PZT films. In the case of $BaTiO_3$ thin films deposited by the laser molecular beam epitaxy method, elongation of *a* and *c* axes has been reported.[22] According to the discussion of this report, the ablated particles with high kinetic energy lead to the interstitial atoms in the growing films, resulting in the compressive stress to the $BaTiO_3$ films. In the case of the sputtering deposition, it could be considered that almost same phenomena should take place. The increase of the cell volume is consistent with the existence of the interstitial atoms induced by the impinging sputtered particles. In WDX measurements, we confirmed the existence of excess Pb in the resulting films, suggesting the excess Pb atoms might be partially settled down in the interstitial position. Alternatively, occupation of Pb atoms in the B site atomic position of the perovskite unit cell may also cause the increase of Pb/(Zr+Ti) ratio and increase of the cell volume because of larger atomic radius of Pb. In the crystallographic analysis using synchrotron radiation, we have successfully confirmed the existence of the Pb atoms in the B site.[23] It can be said that anomalous Pb position like interstitials as well as occupation in B site cause the anomalous crystalline phase diagram of the epitaxial PZT films.

The difference of the crystallographic structure from the bulk ceramics has been reported for the PZT films fabricated by the non-plasma process such sol-gel, MOCVD and the postannealed PZT films,[14–16,24] however, these crystallographic distortion is much smaller than that of the as-grown epitaxial PZT films by sputtering. These results suggest that the energetic sputtered particles play an important roll in the distortion of the PZT crystals because of nonthermally equilibrium reaction such as excess solution of Pb atoms. In this study, the (001)-oriented PZT films of 70/30 exhibited the tetragonal structure with larger *c*-axis spacing (out of plane lattice) than the *a* axis (in plane lattice). The tetragonal PZT films with Zr/Ti composition of 70/30 are attributed to the internal stress induced by the interaction with energetic sputtered particles.

The crystalline structure is also influenced by the orientation of the PZT films as shown in Fig. 4. In particular, the (111)-oriented PZT films of 53/47 and 70/30 exhibited the rhombohedral structure, while (001)-oriented PZT films with the same Zr/Ti composition showed tetragonal phase. For the (001) orientation, the internal stress anisotropically affects the perovskite unit cell between in-plane *a,b* axes and *c* axis, leading to the increase of the c/a ratio. On the other hand, the each axis of perovskite unit is affected by the stress isotropically, resulting in the difference of crystalline structure on the orientation of the films. These assumptions correspond with the fact of the smaller c/a ratio of the (111)-oriented PZT(40/60) films rather than (001)-oriented PZT films.

In the analysis of the electric properties of the PZT films, characteristic dependence on Zr/Ti ratio such as bulk PZT ceramics could not be observed, that is, dielectric and ferroelectric properties were relatively stable with the variation of Zr/Ti ratio. The difference of the electric properties from the bulk values might be attributed to the anomalous crystalline structure of the sputtered epitaxial PZT films. In addition, the internal stress due to the restriction from the substrate as well as the sputter-induced excess Pb in the PZT films should cause the stability of electric properties of the PZT films. As for the P–E hysteresis curves, significant asymmetry was observed, however, this asymmetric curves may be attributed to the existence of charged defects instead of the effect of the distorted crystallinity. Pike *et al.* have reported that the origin of the asymmetric P–E hysteresis is caused by the electric trapping the electric charge trapping due to the oxygen vacancies $V_{o''}$ which are generated by the cooling process of the ferroelectric films in vacuum ambient.[25] In our experiments, the PZT films were also cooled down in vacuum atmosphere after the deposition, therefore it could be considered that the asymmetry of the P–E hysteresis loops is also caused by the oxygen vacancies at the interface of bottom electrode. On the other hand, P_r and E_c of *c*-axis oriented PZT films significantly decreased with increasing Zr/Ti ratio, corresponding to the decrease of the c/a ratio of the PZT unit cell. Thus, the electric properties are influenced by the internal stress due to the sputtering process, however, obvious degradation of dielectric and ferroelectric properties was not observed. These results indicate the deformation of the crystalline structure does not lead to degrade the electric properties, but stabilize them against the variation of Zr/Ti composition.

V. CONCLUSION

In this study, we investigated the crystalline structure of the as-grown PZT films deposited by rf sputtering. Four circle x-ray diffraction measurements revealed that the dependence of crystallographic structure on Zr/Ti ratio was substantially different from those of the bulk ceramics. In particular, (001)-oriented PZT films showed tetragonal structure with the Zr/Ti ratio ranging from 40/60 even to 70/30. Furthermore, epitaxial orientation also affected the crystallographic phase of PZT films. The difference of the crystalline structure of the PZT films between thin films and bulk ceramics might be attributed to the internal stress due to the excess solution of Pb atoms in the films induced by impinging energetic sputtered particles during the deposition. The cell volume of every PZT film also increased, corresponding to the sputter-induced swelling. Dielectric properties of the PZT films exhibit stable dependence of Zr/Ti ratio and characteristic enhancement near Zr/Ti=53/47 could not be observed. These results suggest that the internal stress due to the sputtering deposition plays an important roll in the anomalous characteristics of crystallographic and electrical properties of the epitaxial PZT films.

ACKNOWLEDGMENT

This study was supported by Industrial Technology Research Grant Program in 2002 from New Energy and Industrial Technology Development Organization (NEDO) of Japan.

Downloaded 06 Mar 2008 to 130.54.110.22. Redistribution subject to AIP license or copyright; see http://jap.aip.org/jap/copyright.jsp

[1] J. F. Scott and C. A. Araujo, Science **246**, 1400 (1989).
[2] P. Muralt, A. Kholkin, M. Kohli, and T. Maeder, Sens. Actuators A **53**, 398 (1996).
[3] S. H. Lee, M. S. Jeon, K. I. Hong, J. W. Lee, C. K. Kim, and D. K. Choi, Jpn. J. Appl. Phys., Part 1 **39**, 2859 (2000).
[4] C. R. Cho, L. F. Francis, and M. S. Jang, Jpn. J. Appl. Phys., Part 2 **38**, L751 (1999).
[5] J. G. E. Gardeniers, A. G. B. J. Verholen, N. R. Tas, and M. Elwenspoek, J. Korean Phys. Soc. **32**, S1573 (1998).
[6] I. Kanno, S. Fujii, T. Kamada, and R. Takayama, J. Korean Phys. Soc. **32**, S1481 (1998).
[7] M. Yamamoto, I. Kanno, S. Aoki, Proc. IEEE MEMS 2000, Miyazaki, 2000, p. 217.
[8] S. Hiboux, P. Muralt, and T. Maeder, J. Mater. Res. **14**, 4307 (1999).
[9] E. Cattan, T. Haccart, G. Velu, D. Remiens, C. Bergaud, and L. Nicu, Sens. Actuators A **74**, 60 (1999).
[10] J. F. Shepard, Jr., F. Chu, I. Kanno, and S. Torolier-McKinstry, J. Appl. Phys. **85**, 6711 (1999).
[11] I. Kanno, S. Fujii, T. Kamada, and R. Takayama, Appl. Phys. Lett. **70**, 1378 (1997).
[12] X. Du, U. Belegundu, and K. Uchino, Jpn. J. Appl. Phys., Part 1 **36**, 5580 (1997).
[13] X. Du, J. Zheng, U. Belegundu, and K. Uchino, Appl. Phys. Lett. **72**, 2421 (1998).
[14] S. H. Oh and H. M. Jang, Appl. Phys. Lett. **72**, 1457 (1998).
[15] C. M. Foster, G.-R. Bai, R. Csencsits, J. Vetrone, R. Jammy, L. A. Wills, E. Carr, and J. Amano, J. Appl. Phys. **81**, 2349 (1997).
[16] K. Nagashima, M. Aratani, and H. Funakubo, J. Appl. Phys. **89**, 4517 (2001).
[17] S. P. Alpay, V. Nagarajan, L. A. Bendersky, M. D. Vaudin, S. Aggarwal, R. Ramesh, and A. L. Roytburd, J. Appl. Phys. **85**, 3271 (1999).
[18] S. H. Oh and H. M. Jang, Phys. Rev. B **63**, 132101 (2001).
[19] A. L. Roytburd, S. P. Alpay, V. Nagarajan, C. S. Ganpule, S. Aggarwal, E. D. Williams, and R. Ramesh, Phys. Rev. Lett. **85**, 190 (2000).
[20] G. Shirane and K. Suzuki, J. Phys. Soc. Jpn. **7**, 333 (1952).
[21] E. G. Lee, D. J. Wouters, G. Willems, and H. E. Maes, Appl. Phys. Lett. **69**, 1223 (1996).
[22] T. Zhao, F. Chen, H. Lu, G. Yang, and Z. Chen, J. Appl. Phys. **87**, 7442 (2000).
[23] T. Matsunaga, T. Hosokawa, Y. Umetani, R. Takayama, and I. Kanno, Phys. Rev. B **66**, 064102 (2002).
[24] N. Floquet, J. Hector, and P. Gaucher, J. Appl. Phys. **84**, 3815 (1998).
[25] G. E. Pike, W. L. Warren, D. Dimos, and B. A. Tuttle, Appl. Phys. Lett. **66**, 484 (1995).

Downloaded 06 Mar 2008 to 130.54.110.22. Redistribution subject to AIP license or copyright; see http://jap.aip.org/jap/copyright.jsp